The design and analysis of LED drivers with power factor correction in lighting applications

I. CELİK*, O. FARUK FARSAKOGLU, M. NALBANTOĞLU
Kilis 7 Aralik University, Faculty of Engineering Architecture, Department of Electrical Electronics Engineering, Kilis, 079000, Turkey

Today, light emitting diode (LED) lighting systems are often used in the lighting applications because of their durability, long life and high efficiency. Various important studies have been conducted on LED driver circuits in recent years. Different power converter circuits are often used in LED driver circuits depending on the developments in the power electronics. These circuits both decrease input power factor and lead to high harmonic injection to the circuit. LED driver circuits must conform to the standardization in terms of power factor and harmonics. These standards are to be provided by active power factor correction structures with AC-DC converter. This study mainly classifies single phase power factor correction (PFC) techniques. Based on this classification, passive filters and LED driver circuits with power factor correction were analyzed. It was observed that power factor values to be obtained from passive filter circuits were between 0.448 and 0.93. In addition, power factor correction in the flyback structure with AC-DC converter based was also analyzed. In this respect, a single-phase PFC flyback converter was also designed. This structure was put through discontinuous conduction mode (DCM) simulation and application. Different LED driver power factor (PF), total harmonic distortion (THD) and efficiency rates were observed at different voltage levels. The conformity of LED driver to the international harmonic standards were analyzed using the application results. The results of the analysis suggest that flyback LED driver was more efficient, led to less THD and higher PF compared to passive filter circuits.

(Received June 10, 2016; accepted April 6, 2017)

Keywords: LED lighting, Flyback converter, Power factor correction, Power factor, Total harmonic distortion

Nomenclature

A_e	Cross-sectional area of the core (mm^2)
B_{sat}	Saturation flux density (T)
C_0	Energy storing condenser (F)
D_{MAX}	Maximum operation period (-)
f_{in}	Input frequency (Hz)
f_s	Switching frequency (kHz)
$I_{DS.PK}$	Maximum peak drain current (A)
$I_{DS.RMS}$	Rms drain current of MOSFET (A)
$I_{SW.PK}$	MOSFET peak current (A)
I_{IN}	Average input current (A)
$I_{IN,BNK}$	Input voltage level for V_S blanking (A)
$I_{IN,PK}$	Peak input current (A)
$I_{IN,RMS}$	Rms input current (A)
$I_{OUT,NOM}$	Nominal output current (A)
I_O	Output current (A)
L_{lk}	Leakage inductance (H)
L_m	Transformer's primary-side inductance (H)
N_A	Auxiliary winding (-)
N_E	External winding (-)
N_P	Primer winding (-)
N_S	Seconder winding (-)
N_{AS}	Auxiliary-to-secondary winding turns ratio (-)
N_{AP}	Auxiliary to primary winding turns ratio (-)
N_{PS}	Primary to secondary winding turns ratio (-)
$N_{PMİN}$	Minimum turn number of primary winding (-)
P_{IN}	Input power (W)
P_O	Output power (W)
P_{SN}	Power loss (W)
Q	Active power switch (-)
R_s	Detection resistance value (ohm)
R_{sn}	Snubber resistance (ohm)
t_{DIS}	Inductor current discharge time (s)
t_{ON}	Turn on time (s)
t_S	Switching period (s)
V_A	Auxiliary winding voltage (V)
V_{CE}	Collector-emitter saturation voltage (V)
$V_{CS.PK}$	CS peak voltage (V)
$V_{DS.PK}$	Drain current peak value of the MOSFET (V)
$V_{DS.MAX}$	Maximum drain voltage
V_F	Forward voltage (V)
V_{IN}	Average input voltage (V)
$V_{IN,BNK}$	Input voltage level for V_S blanking
$V_{IN,MIN}$	Minimum input voltage (V)
$V_{IN,MIN.PK}$	Minimum peak input voltage (V)
$V_{IN,MAX}$	Maximum input voltage (V)
$V_{IN,MAX.PK}$	Maximum input peak voltage (V)
V_{OS}	Over voltage in the drain (V)
$V_{OUT,MİN}$	Minimum output voltage (V)
$V_{OUT,MAX}$	Maximum output voltage (V)
V_S	Sensing error (V)
V_{SN}	Snubber capacitor voltage (V)
η	Minimum efficiency (-)

Subscripts

DCM	Discontinuous conduction mode
HFP	High power factor
LED	Ligh Emitting Diode
PFC	Power Factor Correction
PF	Power Factor

1. Introduction

LED lighting systems have been improved due to the technological developments. LED lighting systems use energy quite efficiently. Therefore, LED lighting systems are superior to conventional lighting systems thanks to their ability to reduce environmental hazard in the interaction between energy and environment. In addition, features of LED lights such as long life, high durability and colorful design make these sources indispensable. In recent years, LED lights have been preferred more because of the remarkable decrease in the costs and easy supply. It is estimated that LED lighting systems will replace conventional lighting systems in the near future [1-2].

Important factors such as high efficiency, high power factor and long life must be taken into consideration in the design of a LED driver circuit. Various topological structures are used in order to drive power LEDs. These are divided into three groups as forward resistance, voltage regulator and DC-DC converter circuits [3-5].

In general, the structure of a LED driver circuit consists of a bridge rectifier, a DC-DC converter and a DC link capacitor between them. However, this structure cases a low power factor and high total harmonic distortion. Therefore, power factor rectifiers are used in different structures. The first one is passive filter structures, which are the most basic power factor rectifiers. It is not likely to conform to IEC-61000-3-2 standards and high power factor with these structures. Thus, a more complex structure is needed in terms of the bridge rectifier [6].

The structure with two power transformation stages, which is shown in Fig. 1, is used to rectify power factor. In this two-stage LED driver, the first stage consists of a transform which can shape an AC-DC input current in terms of power factor while the second stage consists of a DC-DC converter. Two-stage PFC structure are controlled by two independent controllers. As a result, the complexity and cost of PFC circuits increase and they are not used in low power applications [7].

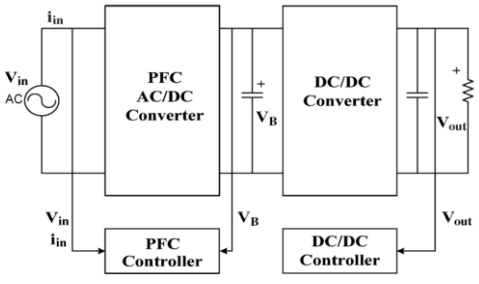

Fig. 1. Two stage HPF power factor correction

In a single stage power factor correction circuit, a single controller both rectifies the power factor and regulates the output voltage. The single controller is of vital importance for a simpler and cost-effective circuit. Therefore, LED driver circuits with a single stage power factors are preferred due to their easy controlling and low cost compared to two-stage circuits [8]. State-of-the-art LED drivers using the single-stage PFC topology have been published in [9–11].

For general lighting applications, harmonic components of a LED driver of 25 W and higher must comply with the IEC 61000-3-2 class C standards and remain within the defined limits [12,13]. Therefore, various single stage PFC circuits are developed in order to increase power factor. The most commonly used among these circuits is the single stage flyback structure [14-17]. A high power factor is obtained from these converters because input current is a rectified sine wave and in the same phase with the input current. The single stage flyback structure usually operates in the DCM. This study focuses on single stage flyback power factor correction circuit which is used for LED lighting applications at different power levels. The single stage flyback circuit operates in DCM. The power factor and total harmonic components of this circuit for different power levels, and its conformity to IEC 61000-3-2 class C standards and the defined limits were analyzed. Additionally, the efficiency of single stage flyback structure at different power levels were also analyzed.

2. Methods

Single phase PFC methods in LED driver circuits are divided into two groups: LED drivers with passive PFC and LED drivers with active PFC.

2.1. LED drivers with Passive Filter

Power LEDs need fixed current in order to emit light, which requires different driver circuits. The circuit diagrams of forward resistance and voltage regulator circuits are shown in Fig. 2a and 2b.

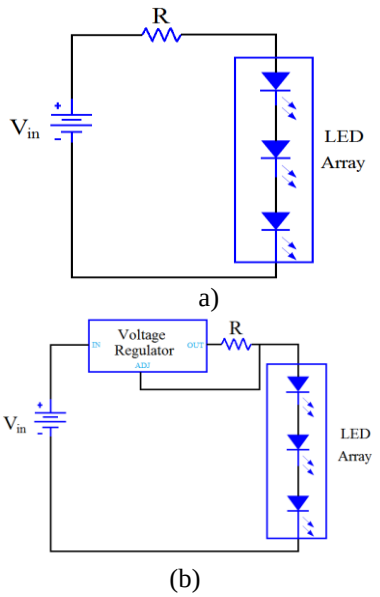

Fig. 2. a) Forward resistance LED driver
b) linear LED driver

In these circuits is converted DC voltage through passive elements and bridge rectifier. In the passive PFC circuits, power factor correction is performed by changing the circuit structure. This section deals with LED drivers without PF correction and PF methods for these structures.

- LED drivers without power factor correction (Type 1)
- Inductive power factor correction (Type 2)
- Series resonant filter power factor correction (Type 3)

2.1.1. LED drivers without power factor correction

LED driver circuits with full wave rectifier and condenser filter are shown in Fig. 3.

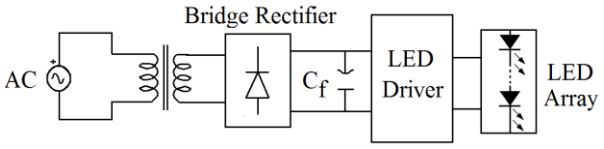

Fig. 3. A LED driver without power factor correction

The irregularity in the output voltage of the bridge rectifier is preserved at a minimum level. Therefore, C_f capacitor in the output is maximized. A current is transmitted to the condenser at a point where the grid voltage is at maximum. The load is fed by the condenser in the rest of the period. The energy needed is provided from the current that transmitted in a short time at the grid. High harmonic currents are transmitted to these circuits from the grid [18]. Therefore, they lead to inefficient power quality and coefficient.

2.1.2. Inductive power factor correction

The LED driver with power factor correction with an inductor on DC-side, which is created by adding an inductor on the DC-side of the bridge rectifier, is shown in Fig. 4.

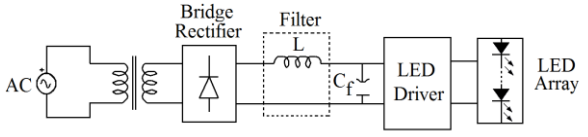

Fig. 4. The LED driver with power factor correction with an inductor on DC-side

It is one of the most basic structures. Its highest power factor may reach 0.765 [19].

2.1.3. Series resonant factor power factor correction

The form of the current transmitted by the grid can be altered by using low pass filter combinations in the input and output. A series resonant filter used for PFC is shown in Fig. 5. L-C frequency filter is designed to allow basic frequency component and avoid harmonic components. Large scale reactive elements will be needed in these filters for 50 Hz grids, which helps obtain higher power factor values [20].

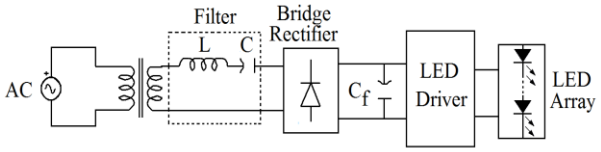

Fig. 5. LED driver with series resonant filter power factor correction

2.2. Flyback led driver with active power factor correction

Switching devices such as MOSFET and IGBT are used in active PFC methods in order to shape the power line current. It is possible to make power factor reach one by controlling the power amount transmitted to the load because of semi-conductor switches present in a switched mode power supply. This section focuses on the fundamental operation of the flyback converter and its design process.

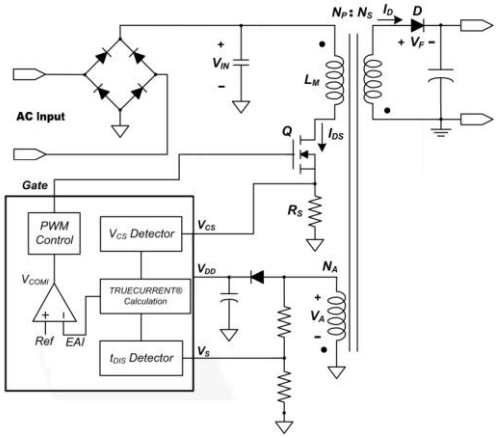

Fig. 6. Flyback converter based active power factor c orrection circuit [22]

The flyback converter structure is a DC-DC converter based power factor correction circuit which enables isolation between the rectified AC grid voltage and LED series as shown in Fig. 6.

The voltage polarization between primary and secondary windings are shown with dots in this figure.

L_m denotes the magnetic inductance of the transformer. When the active power switch Q is turned out input power is stored in the L_m inductance, meanwhile the Q switch is turned off power is transferred the load. C_0, the

energy storing condenser, is an electrolytic condenser which is used to supply a stable DC voltage to the LED armature. In the flyback transformer, it can be operated in the continuous conduction mode or discontinuous conduction mode in terms of the continuity of primary winding current. When Q, the active power switch, is switched, a vibrant wave occurs in the input current at the same frequency. The length and amplitude of vibrant wave is controlled by a suitable method, and the mean input current may converge the sine wave and may occur in the same phase as the input voltage, which leads to a power factor closer to one and a very low total harmonic distortion. The wave forms of the flyback transformer operating in the discontinuous conduction mode is shown in Fig. 7 [21,22].

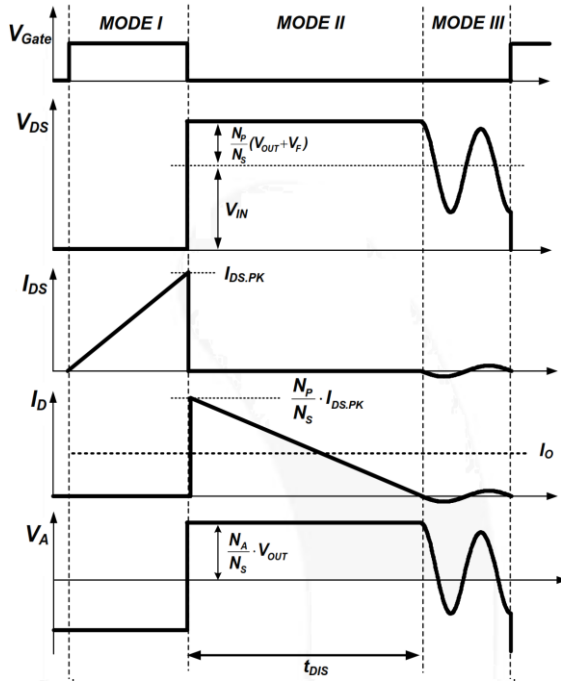

Fig. 7. The wave forms of the flyback transformer operating in the discontinuous conduction mode [18]

Single-stage flyback LED driver was designed for FL7733A. Some assumptions were made in this design process, and the transformer primary side inductance (L_m), detection resistance (R_s), primary secondary winding turn ratio (N_{PS}), auxiliary to secondary winding turn ratio (N_{AS}), auxiliary to primary winding turn ratio (N_{AP}), V_s circuit, the selection of MOSFET and the design of RCD snubber circuit were performed.

First step: Selecting the inductance of transformer primary side

The operation of FL7733A integrated at fixed turn on time and constant turn off time is shown in Fig. 8. The turn on time (t_{ON}) and switching period (t_S) of MOSFET is fixed. It is possible to obtain higher power factor when the average input current (I_{IN}) is proportional to the average input voltage (V_{IN}).

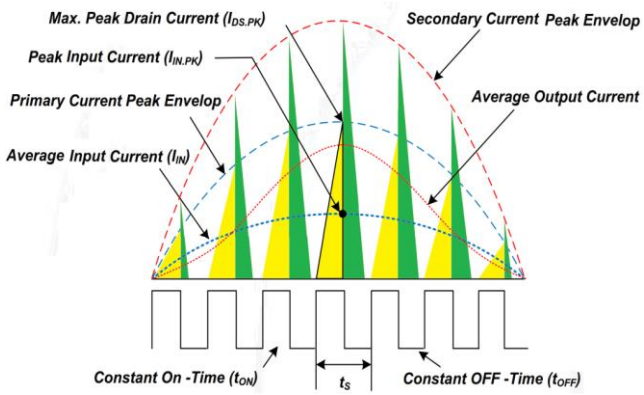

Fig. 8. Theoretical wave forms [22]

The single stage flyback structure in this study was used along with FL7733A integration. Because this structure possesses fixed transmission and break time, it is assumed to operate in the discontinuous conduction mode. The input voltage is applied to the magnetic coil (L_m) while the switch is in transmission. Therefore, the maximum peak drain current ($I_{DS,PK}$) of the MOSFET occurs at the peak point of the voltage. $I_{DS,PK}$ current of MOSPET in the minimum input voltage and full load is calculated as follows.

$$I_{DS,PK}=\frac{t_{ON}\times V_{IN,PK}}{L_m}, \tag{1}$$

Here, $V_{IN,PK}$ represents the input voltage peak value, and t_{ON} represents the maximum turn on time in the minimum input voltage. The peak input current is obtained via Equation 1 as follows.

$$I_{IN,PK}=\frac{1}{2}\times(t_{ON})\times\left(\frac{V_{IN,PK}}{L_m}\times t_{ON}\right)\times f_s, \tag{2}$$

$I_{IN,PK}$ and $V_{IN,PK}$ are defined in Equation (3) and (4). Here, $I_{IN,RMS}$ and $V_{IN,RMS}$ denote the active value of input voltage and current.

$$I_{IN,PK}=\sqrt{2}\times I_{IN,RMS}, \tag{3}$$

$$V_{IN,RMS}=\sqrt{2}\times V_{IN,RMS}, \tag{4}$$

t_{ON} length must be calculated in order to calculate L_m value. For this purpose, t_{ON} is calculated via Equation 2 and 4 as follows.

$$t_{ON}^2=\frac{2\times L_m\times I_{IN,RMS}}{V_{IN,RMS}\times f_s}. \tag{5}$$

Input power is defined as follows,

$$P_{IN} = V_{IN,RMS} \times I_{IN,RMS} = \frac{P_o}{\eta}, \quad (6)$$

Here, P_o represents the output power.

L_m value is obtained via Equation 5 and 6 as follows [22].

$$L_m = \frac{\eta \left(V_{IN,RMS}\right)^2 f_s t_{ON}{}^2}{2P_o}. \quad (7)$$

Second step: Detection resistance (R_s) and the rate of primary secondary winding (N_{PS})

Output current is directly proportional to N_{PS} conversion rate between primary and secondary windings of the transformer, and inversely proportional to the detection resistance (R_s). V_{CS} is determined in order to avoid short circuit or excessive load in the system and FL7733A is used to limit the current in each period. V_{CS} is usually adjusted to 0.85V. MOSFET peak current ($I_{SW,PK}$) is converted to a voltage as $V_{CS,PK}$ as shown in the following equation.

$$V_{CS,PK} = I_{SW,PK} \times R_S, \quad (8)$$

$$I_o = 0.125 \times \frac{N_p}{N_s} \times \frac{1}{R_s}, \quad (9)$$

The relationship between the rate of primary secondary winding and output current and detection resistance is defined via Equation 9 as follows [22].

$$N_{PS} = \frac{I_O \times R_S}{0.125}. \quad (10)$$

Third step: The conversion rate of auxiliary and secondary winding (N_{AS}) and the conversion rate of auxiliary and primary winding (N_{AP})

The operation range of FL7733A integration is between 8.75V and 23V. When it is 23V, V_{DD} stops switching because of over voltage protection (OVP). Here, N_{AS} and N_{PS} rates are defined as follows [22].

$$N_{AS} = \frac{V_{DD,OVP}}{V_{O,OVP}} = \frac{23}{V_{O,OVP}}, \quad (11)$$

$$N_{AP} = \frac{N_{AS}}{N_{PS}}, \quad (12)$$

Fourth Step: Transformer design and Vs circuit

The number of primary windings is determined based on Faraday law. $N_{P,MIN}$ primary winding is fixed based on the peak value of the minimum grid input voltage ($V_{IN,MIN.PK}$) and maximum transmission time. In order to prevent the core on the primary side of the transformer from saturation, $N_{P,MIN}$, which is the minimum number of windings, and N_E, which is the number of external windings, are defined via the formulas below [23].

$$N_{P,MIN} = \frac{V_{IN,MIN.PK} \times t_{on}}{B_{sat.} \times A_e}, \quad (13)$$

$$N_E = \frac{(8.75 + V_{CE,Q1} + V_{F,D3})}{\left(V_{F,D0} + V_{MIN,OUT}\right)}, \quad (14)$$

In this formula, as far as the minimum output voltage is concerned, $V_{CE,Q1}$ represents the collector emitter saturation voltage of Q_1, $V_{F,D3}$ represents the forward voltage of D_3 and $V_{F,D0}$ represents the forward voltage of D_0.

For Vs circuit, the first step that must be taken into consideration in the selection of R_{14}, R_{15} voltage is that the diode current of V_s voltage must be 2.45 at the end of transmission time in order for the system to operate at a switching frequency of 65 kHz in the nominal power. The second important point is the V_s voltage.

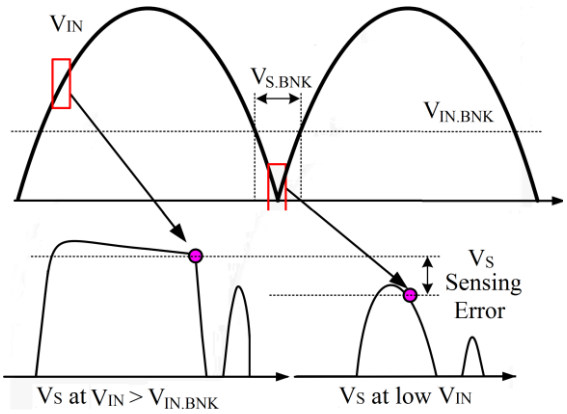

Fig. 9. V_S wave form [18]

V_S should be kept between 0.6 and 3 V for wide output voltage applications. As shown in Fig. 13, this can be achieved via an additional Vs circuit. R_{14} and R_{15} voltage values in this circuit are defined as follows [22].

$$R_{14} = N_{AP} \times \frac{V_{IN,BNK}}{I_{VS,BNK}}, \quad (15)$$

In this equation, $V_{IN,BNK}$ represents the sampling input line voltage meanwhile $I_{VS,BNK}$ stands for current level for sampling input line voltage in Fig. 9. R_{15} voltage is calculated as follows [22].

$$R_{15} = \frac{R_{14} \times 2.45}{V_{sc} - 2.45}. \quad (16)$$

Fifth step: MOSFET selection

MOSFET drain voltage is analyzed in the determination of winding ratio of the transformer. When the over voltage in the drain is defined as V_{OS}, maximum drain voltage is defined as follows.

$$V_{DS(MAX)} = V_{IN,MAX.PK} + \frac{N_p}{N_s}(V_{o,ovp} + V_{F,D0}), \quad (17)$$

Here, $V_{in,max.tp}$ represents the maximum peak input voltage. Rms current of MOSFET is calculated as shown in equation (18).

$$I_{DS,RMS} = I_{PK} \times \sqrt{\frac{t_{ON} \times f_S}{6}}, \quad (18)$$

The voltage and current values of the selected MOSFET must exceed these values based on a safety coefficient.

Sixth step: RCD Snubber circuit design

A break in the power MOSFET of single stage flyback LED driver circuit may lead to sudden voltage increases in the drain due to the leakage inductance in the transformer. This over voltage on the MOSFET creates a avalanche current effect and harms the device. Therefore, an additional circuit must be used to reduce the voltage. A similar RCD snubber circuit and its wave form are shown in Fig. 10 [22-24].

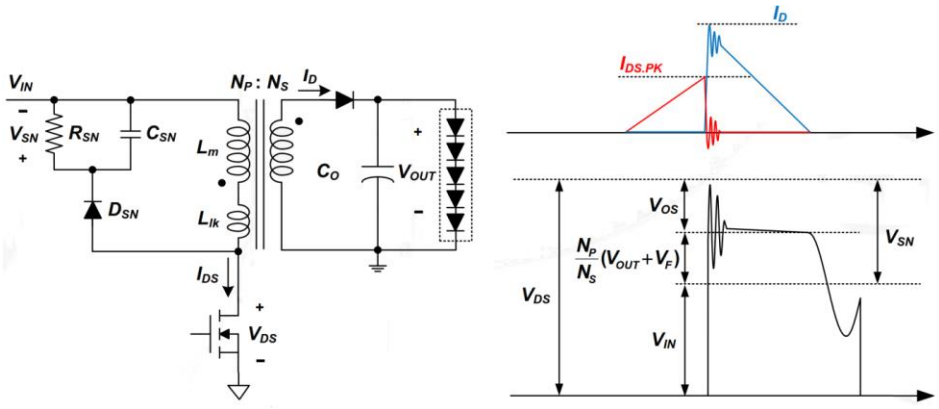

Fig. 10. Snubber circuit and wave forms [22]

When MOSFET drain voltage exceeds cathode voltage of the snubber diode, snubber diode starts transmission and absorbs the leakage inductance current. When snubber circuit is analyzed, the snubber capacitor voltage is assumed to possess such a capacity that it does not change during a switching period. The full-load snubber capacitor voltage is defined as follows.

$$V_{SN} = V_{RO} + V_{OS}. \quad (19)$$

Power loss in the snubber circuit is expressed as follows.

$$P_{SN} = \frac{V_{SN}^2}{R_{SN}} = \frac{1}{2} L_{lk} \times I_{DS,PK}^2 \times \frac{V_{SN}}{V_{SN} - V_{RO}} \times f_s, \quad (20)$$

Here, L_{lk} represents leakage inductance, V_{sn} represents full load snubber capacitor voltage and R_{sn} represents snubber resistance. The maximum volatility in the snubber capacitor voltage is defined as follows.

$$\Delta V_{SN} = \frac{V_{SN}}{C_{SN} \times R_{SN} \times f_s} \quad (21)$$

A capacitor which will cause a voltage ripple between 5% and 20% is usually preferred.

3. Analysis and discussion

This section displays results obtained from the simulation and application of passive filter LED drivers and active power factor correction flyback structures. As for LED drivers with passive filter power factor correction, the values of elements used in the circuits in PROTEUS program for the conditions under which AC input voltage is 220 V and there are 8 pieces of LEDs connected in series in the output are given in Table 1.

Table 1. Values of elements in passive filter power factor correction structures

	Method	I_{in} (A)	G.F	THD (%)	Efficieny (%)
Forward resistance	TYPE 1	0.43	0.45	198.14	51.36
	TYPE 2	0.22	0.73	49.2	61.95
	TYPE 3	0.18	0.93	19.47	58.7
Voltage Regulator	TYPE 1	0.43	0.45	198.2	51.36
	TYPE 2	0.22	0.72	49	62.13
	TYPE 3	0.18	0.93	18.4	59.11

The simulation studies related to the different power factor correction methods used in the LED driver circuits with forward resistance and voltage regulators, which were discussed in Section 2.1, were performed in PROTEUS. The results of these simulation studies are given in Table 2. It was observed in these circuits that power factor is between 0.448 and 0.937, total harmonic distortion is between 198.14% and 18.4%, and efficiency is varied between 51.36% and 62.13%.

Table 2. Simulation results of passive filtered power factor correction structures

	Method	R (Ω)	L (mH)	C (mF)	C_f (mF)
Forward resistance	TYPE 1	37.9	-	-	4.71
	TYPE 2	22.4	15	-	4.71
	TYPE 3	24.2	102	82	4.71
Voltage Regulator	TYPE 1	1.78	-	-	4.71
	TYPE 2	1.78	15	-	4.71
	TYPE 4	1.78	102	82	4.71

It can be inferred from Table 2 that power factor and total harmonic distortion of Type 1 and Type 2 with forward resistance do not conform to the standards of IEC 61000-3-2 class C while Type 3 with forward resistance conforms to the same standards. The analysis of total harmonic component of Type 3 with forward resistance based on its input current and voltage data analysed in MATLAB is shown in Fig. 11. It can be observed from the structures with forward resistance that their efficiency rates are 51.36%, 58.7% and 61.95%.

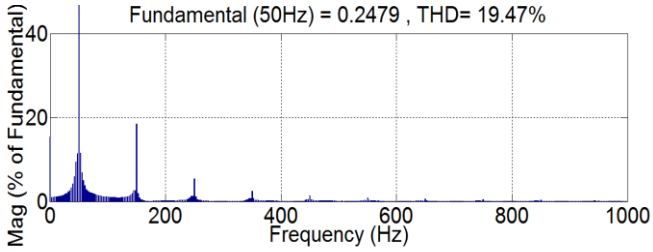

Fig. 11. Harmonic components in proportion to basic component

It can be inferred from Table 2 that Type 1 and Type 2 with voltage regulator do not conform to the standards of IEC 61000-3-2 class C because their power factor is low and total harmonic distortion is quite high. It is observed that total harmonic distortion of Type 3 with voltage regulator is 18.39%. The analysis of total harmonic component of Type 3 with voltage regulator is shown in Fig. 12. It can be observed from Table 2 that the efficiency rates of Type 1, Type 2 and Type 3 are 51.36%, 62.13% and 59.11%, respectively.

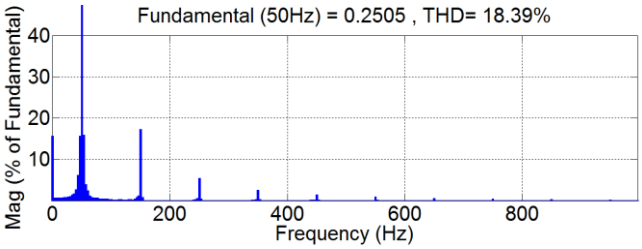

Fig. 12. Harmonic components in proportion to basic component

Parameters of Flyback converter LED driver with HPF, which is an active filter structure, designed in this study are given in Table 3.

Table 3. Design parameters of LED driver with HPF

Parameters		Symbol	Value	Unit
Input	Voltage	$V_{IN,MIN}$	90	Volt
		$V_{IN,MAX}$	305	Volt
	Frequency	f_{in}	50	Hz
Output	Voltage	$V_{OUT,MİN}$	25	Volt
		$V_{OUT,MAX}$	55	Volt
	Frequency	$I_{OUT,NOM}$	0.58	Amper
Switching frequency		f_s	65	KHz
Maximum operation period		D_{MAX}	% 40	
Minimum efficiency		η	% 88	

For $V_{CS,PK}$ 0.85 V, RM10 core between N_P 5% and 10%, when equations 1-21 given in Section 2 are used, calculations were based on $V_{F,D0}$ 1 V, $V_{CE,Q1}$ 0.5 V, $V_{F,D3}$ 0.7 V, V_{OS} = 100 V, V_{SN} = 200 V, ΔV_{SN} is 5%, and L_{lk}=3µH. Various important parameters of Flyback LED driver with HPF based on this calculation are given in Table 4.

Table 4. Important parameters of Flyback LED driver.

L_m (µH)	$I_{DS,P}$ (A)	R_s (Ω)	N_{PS}	N_P	N_S
293	2.68	0.32	1.5	29.5	22
N_A	N_E	R_2 (kΩ)	R_3 (kΩ)	R_{SN} (kΩ)	C_{SN} (nF)
9	3	151.15	$R_3 \geq 47.51$	33.33	10

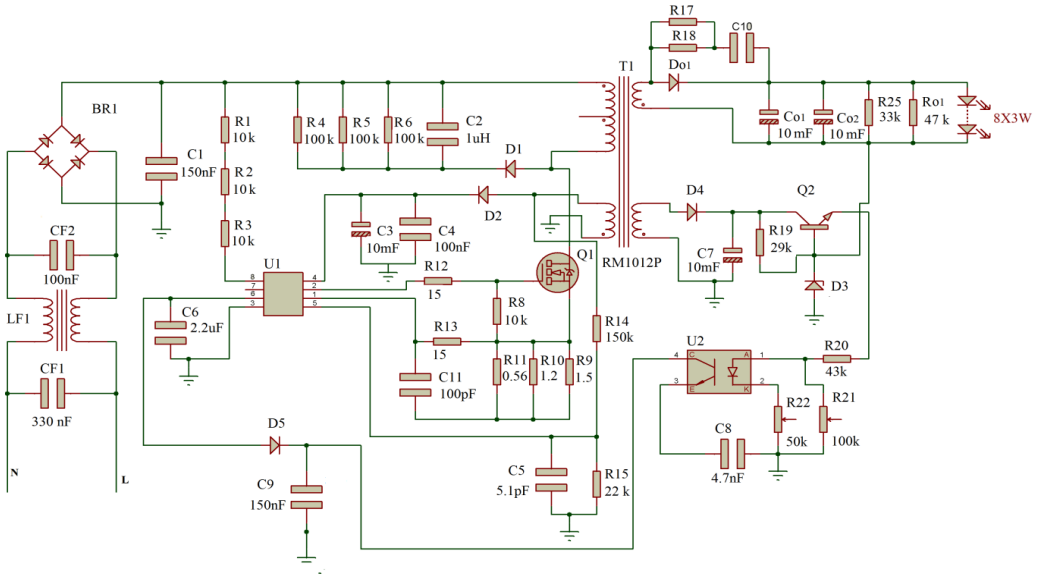

Fig. 13. The circuit diagram of Flyback LED driver with HPF

The circuit diagram of Flyback LED driver with HPF, shown in Fig. 13. Wave forms of input current and input voltage obtained from the simulation studies carried out with 220 V input voltage are shown in Fig. 14.

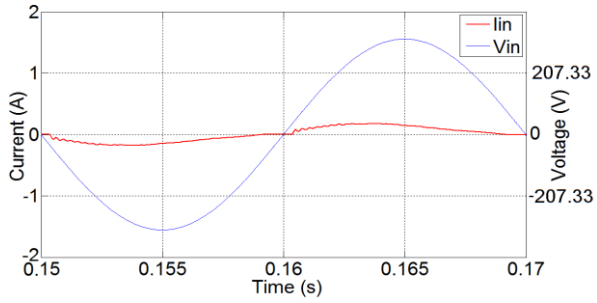

Fig. 14. Wave forms of input current and voltage of LED driver with HPF in the simulation

Power factor is 0.93 and total harmonic distortion is 18.07% for the input current and voltage are shown in Fig. 14. Harmonic spectrum of the input current is shown in Fig. 15.

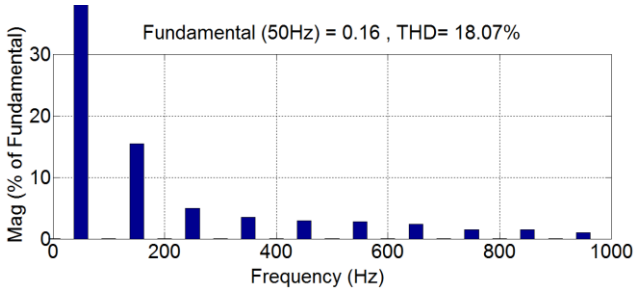

Fig. 15. Harmonic components in proportion to basic component

Output current and voltage changes obtained from the simulation studies carried out for this structure are given in Fig. 16. It can be observed that the mean output voltage is 30.2 V and output current is 590 mA.

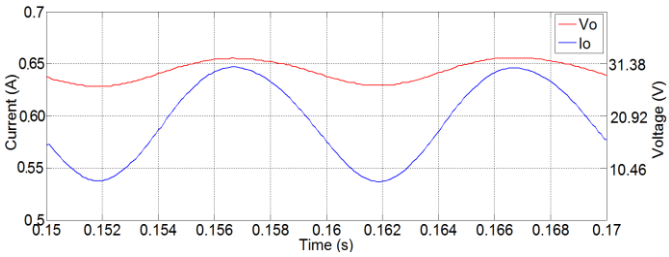

Fig. 16. Wave forms of output current and voltage of Flyback simulation

The application circuit of Flyback LED driver with HPF, shown in Fig. 17, was performed, and its input and output waveforms were noted.

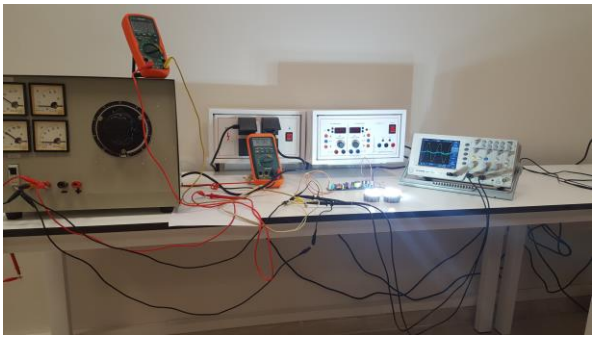

Fig. 17. Flayback LED driver application circuits

Oscilloscope images of input current and voltage waveforms obtained from application results are shown in Fig. 18. There is a phase difference of 22º between input current and input voltage. Harmonic spectrum of the input current is shown in Fig. 19.

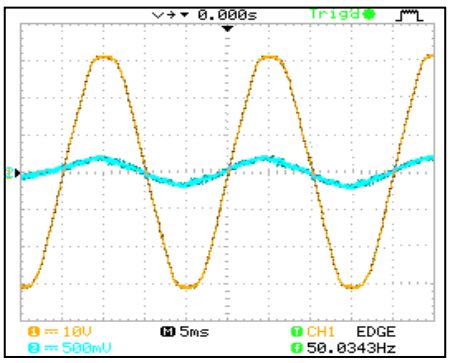

Fig. 18. Wave forms of input current and voltage of application circuits with 220 V input voltage

The results of applicationis based on input current and voltage data suggest that power factor and total harmonic distortion are 0.928 and 15.71%, respectively.

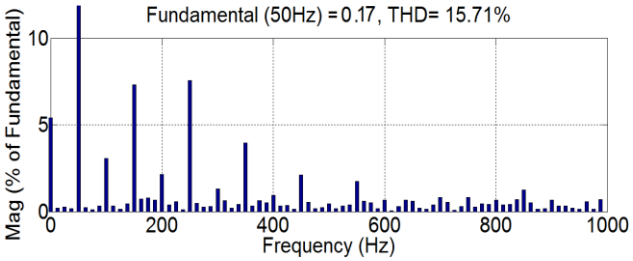

Fig. 19. Harmonic components in proportion to basic component

Output current and voltage changes based on application results are shown in Fig. 20. The mean output voltage is 30.6 V and mean output current is 576 mA. A slight fluctuation can be observed in output current and voltage as shown in Fig. 20. The ripple in the output current is 100 mA while it is 3 V in the output voltage.

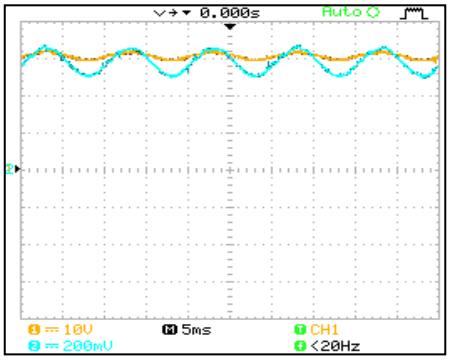

Fig. 20. Wave forms of output current and voltage of application circuits with 220 V input voltage

The application of Flyback LED driver with 90V input voltage was performed, and its input and output waveforms were noted. Oscilloscope images of input current and voltage waveforms are shown in Fig. 21.

There is a phase difference of 8,1º between input current and input voltage.

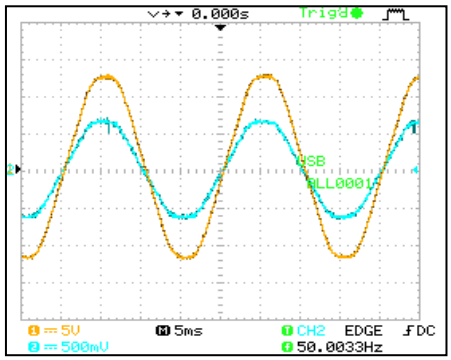

Fig. 21. Wave forms of input current and voltage of application circuits with 90 V input voltage

Output current and voltage wave forms are shown in Fig. 21. The mean output voltage is 30.6 V and mean output current is 576 mA. The ripple in the output current is 100 mA while it is 3 V in the output voltage.

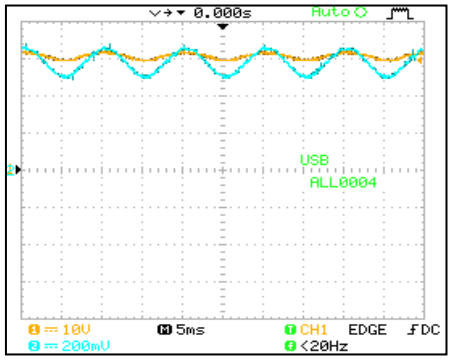

Fig. 22. Wave forms of output current and voltage of application circuits with 90 V input voltage

Harmonic spectrum of the input current is shown in Fig. 23.

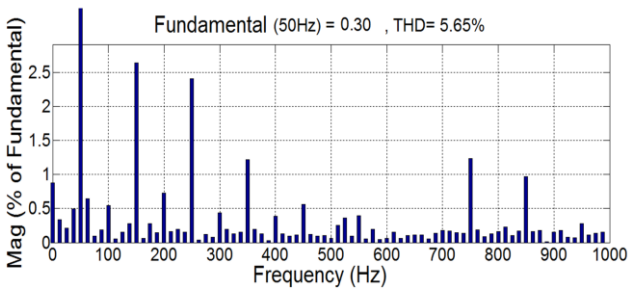

Fig. 23. Harmonic components in proportion to basic component

The results of application based on input current and voltage data suggest that power factor and total harmonic distortion are 0.99 and 5.65%, respectively.

Table 5. Application results at different voltage levels

V_{inrms} (V)	I_{inrms} (mA)	V_{LED} (V)	I_{LED} (mA)	P_{out}(W)	P_{in}(W)	Efficiency (%)	PF	THD%
90	225.7	30.6	576	17.63	20.11	87.6	0.99	5.65
120.43	166.2	30.6	576	17.63	19.78	89.1	0.988	6.32
150	137.7	30.6	576	17.63	20.1	87.7	0.973	9.73
180.14	114.2	30.6	576	17.63	19.54	90.2	0.95	11.59
220	96.6	30.6	576	17.63	19.72	89.4	0.928	15.71

Flyback LED driver was operated at 24 W, and data on input current (I_{in}), output current (I_{LED}), output voltage (V_{LED}), power factor (PF), total harmonic distortion (THD) and efficiency of LED driver are given in Table 5. LED driver was operated at five different voltage levels.

As it can be observed in Table 5 that the efficiency of flyback LED driver with HPF is high and that it conforms to the standards of IEC 61000-3-2 class C. The findings suggest that with 220 V input voltage and its harmonic components are quite low compared to the values specified in these standards as seen in Fig. 24.

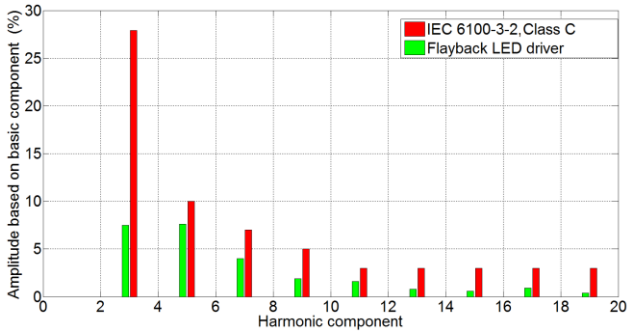

Fig. 24. Harmonic components in proportion to basic components

4. Conclusion

This study aimed to improve the power quality of a LED driver circuit when its AC input voltage varies between 90V and 220V and provide a more efficient energy consumption.

In this context, the present study firstly dealt with passive filter power factor correction circuits. Simulation studies were performed on a structure which input voltage was 220 V and 8 pieces of LEDs were connected in series in the output. Simulation results demonstrated that the power factor of these passive filter circuits varied between 0.448 and 0.93, their total harmonic distortion varied between 198.14% and 17.84%, and their efficiency rates varied between 51.36% and 62.13%. Passive filter LED driver circuits offer advantages such easy and safe usage, durability, insensitivity to voltage fluctuation and noise, preventing electromagnetic interference (EMI) and does not have high frequency switching losses. However, it was understood that these circuits did not meet the standards of IEC 61000-3-2 class C.

Secondly, in this study LED driver circuit with HPF, which is one of the active power factor correction applications, was analysed and its working principle was examined. Afterwards, for an input voltage range of 90 and 220 V, the design parameters of a circuit which output voltage was between 25 and 55 V and output current was 576 mA were determined. The designed LED driver circuit was simulated when there are eight series LED load in the output. Experiments were performed on this circuit for five different voltage levels. Data on input current (I_{in}), output current (I_{LED}), output voltage (V_{LED}), power factor (PF), total harmonic distortion (THD) and efficiency of LED driver were obtained. It was found out that simulation studies yielded a total harmonic distortion of 18.07% and power factor of 0.93 when AC input voltage is 220 V. On the other hand, application results demonstrate that total harmonic distortion and power factor are 15.71% and 0. 928, respectively. In other words, the simulation results overlapped the application results. But THD result in application is lower than result in the simulation. Because variac voltage regulator inductance affected THD value in application.

In conclusion, single stage flyback LED drivers provided high power factor and low total harmonic distortion. It was observed that harmonic components of the input current conform to the standards of IEC 61000-3-2 class C. In addition, due to designs are performed in accordance with the international standards, flyback LED driver circuits offered higher efficiency for medium and high lighting application in where AC input voltage is high.

References

[1] A. Shrivastava, B. Singh, S. Pal, IEEE Transactıons On Industrıal Electronıcs **62**(10), 6272 (2015).

[2] H. L. Cheng, C. A. Cheng, C. S. Chang, Proceeding of IEEE 2nd International Symposium on Next-Generation Electronics (ISNE), 146 (2013).

[3] O. F. Farsakoğlu, I. Çelik, I. Atik, H. Y. Hasırcı, Proceeding of Second International Symposıum on Engineering Artifical Intelligence& Applications, 133 (2014).
[4] O. F. Farsakoğlu, I. Atik, Optoelectron. Adv. Mat. **9**(11-12), 1356 (2015).
[5] O. F. Farsakoğlu, H. Y. Hasırcı, J. Optoelectron. Adv. Mat. **17**(5-6), 816 (2015).
[6] H. Ma, J. S. Lai, Q. Feng, W. Yu, C. Zheng, Z. Zhao, IEEE Transactıons on Power Electronıcs **27**(6), 3057 (2012).
[7] R. G. Alireza, S. M. Javad, A. Babak, in proceeding of 4th Power Electronics, Drive Systems & Technologies Conference (PEDSTC2013), 218 (2013).
[8] Q. T. Nha, M. M. Alam, in Proceeding of Anti-Counterfeiting, Security and Identification 1 (2012).
[9] D. G. Lamar, J. S. Zuniga, A. R. Alonso, M. R. Gonzalez, M. M. H. Alvarez, IEEE Trans. Power Electron. **24**(8), 2032 (2009).
[10] H.-J. Chiu, Y.-K. Lo, J.-T. Chen, S.-J. Cheng, C.-Y. Lin, S.-C. Mou, IEEE Trans. Ind. Electron. **57**(2), 735 (2010).
[11] Q. Hu, R. Zane, IEEE Trans. Power Electron. **25**(3), 574 (2010).
[12] Limits Electromagnetic Compatibility (EMC)—Part 3-2: Limits for Harmonic Current Emissions (Equipment Input Current ≤16 A per Phase), Edition 2.1, IEC Standard 610 00-3-2, Oct. 2001.
[13] Y. Hu, L. Huber, M. M. Jovanović, in Proceeding of Industry Applications Society Annual Meeting 1 (2009).
[14] X. Xie, J. Wang, C. Zhao, Q. Lu, S. Liu, IEEE Transactıons On Power Electronıcs **27**(11), 4602 (2012).
[15] D. G. Lamar, M. Arias, A. Rodríguez, A. Fernández, , M. M. Hernando, J. Sebastián, J. E. Yeon, D. S. Kim, K. Cho, H. J. Kim, IEEE Transactıons On Industrıal Electronıcs **60**(7), 2614 (2013).
[16] J. J. Lee, J. M. Kwon, E. H. Kim, W. Y. Choi, B. H. Kwon, IEEE Transactıons On Industrıal Electronıcs **55**(3), 1352 (2008).
[17] H. Chiu, H. Huang, H. Yang, S. Cheng, Int. J. Circuit Theor. Appl. **36**(2), 205 (2008).
[18] S. Basu, Ph.D. thesis (Chalmers Uni., Sweden), 2006.
[19] G. Yanık, MSc thesis, (Yıldız Teknik Uni.,Turkey), 2010.
[20] A. G. Vishal Anand, Ms.C thesis (Indian Institute of Science Uni., India), 2005.
[21] Y. C. Chuang, Y. L. Ke, H. S. Chuang, C. C. Hu, in Proceeding of IEEE Industry Applications Society Annual Meeting 1 (2010).
[22] Application notes. (2016, May 13). Retrieved from https://www.fairchildsemi.com/application notes/AN/AN-5076.pdf.
[23] Application notes. (2016, May 13). Retrieved from https://www.fairchildsemi.com/application-notes/AN/AN-4140.pdf.
[24] P. Meng, X. Wu, J. Yang, H. Chen, in Proceeding of Power Electronics Conference and Exposition 642 (2010).

*Corresponding author: ibrahimcelik@kilis.edu.tr